Mathematics and Computers in Simulation 225 (2024) 648–658

Contents lists available at ScienceDirect

Mathematics and Computers in Simulation

journal homepage: www.elsevier.com/locate/matcom

Original articles

In silico investigation of the formation of multiple intense zebra stripes using extending domain

Hyundong Kim [a], Jyoti [b], Soobin Kwak [c], Seokjun Ham [c], Junseok Kim [c,*]

[a] Department of Mathematics and Physics, Gangneung-Wonju National University, Gangneung 25457, Republic of Korea
[b] The Institute of Basic Science, Korea University, Seoul 02841, Republic of Korea
[c] Department of Mathematics, Korea University, Seoul 02841, Republic of Korea

ARTICLE INFO

Keywords:
Turing pattern
Extending domain
Multiple intense zebra stripe formation

ABSTRACT

We perform an *in silico* investigation of the formation of multiple intense zebra stripes by extending the domain with an appropriate extending speed. The common zebra has alternating dark and light stripes, creating a two phase pattern. However, some Equus burchelli zebras have an intermediate gray color stripe situated between the dark and light stripes. To numerically investigate the formation of multiple intense zebra stripes, we first find the equilibrium state of the governing system in the one-dimensional (1D) static domains using various frequency modes. After finding the equilibrium state for the governing system in the 1D static domains, we stack a numerical data. Then, we load the stacked numerical data to use as an initial state for finding the growth rate that forms the multiple intense zebra stripe formation in the 1D extended domains. Next, convergence experiments are conducted to verify the convergence of the numerical method for the governing system. Finally, numerical simulations are performed to confirm the formation of multiple intense zebra stripes in two-dimensional extending domains and on evolving curved surfaces.

1. Introduction

After C. Darwin theorized about the benefits of zebra stripes [7,22], numerous scientists have conducted research to confirm or refute his assertions. Previously, it was believed that zebras' stripes helped them to camouflage from predators. However, recent scientific findings suggest that these stripes may primarily serve as protection against biting flies such as the tsetse fly [5,26]. These flies are carriers of diseases such as anthrax and trypanosomiasis, which can be fatal to zebras. The stripes may confuse the flies, making it difficult for them to land on zebras and bite them. Zebra stripe patterns help to protect the zebras from disease and allow them to live longer and healthier lives. Research on zebra stripes and their relationship with biting flies is ongoing, and scientists are still gaining insights into the complete extent of the stripes' protective benefits. There are three primary zebra species, namely Equus burchelli, Equus zebra, and Equus grevyi [11]. The patterns of stripes in different species of zebras evolve with distinct numbers and sizes over time [2]. Among them, the shadow stripe that emerges on some Equus burchelli zebra skin [4,5] is an interesting topic of research in the fields of mammalian and mathematical biology. The formation of shadow stripe patterns in Equus burchelli zebra skin is manifested by rapid growth effects when growing from an embryonic state to adulthood [11]. In zebras, this occurs very early (between 21–35 days), while their gestation period is approximately 360 days. Moreover, before color cells are fully expressed, these shadow stripes are formed on zebra skin by rapid growth during the formation of dark and white stripe patterns [11].

* Corresponding author.
E-mail addresses: hdkim@gwnu.ac.kr (H. Kim), cfdkim@korea.ac.kr (J. Kim).
URL: https://mathematicians.korea.ac.kr/cfdkim (J. Kim).

https://doi.org/10.1016/j.matcom.2024.06.010
Received 16 November 2023; Received in revised form 11 April 2024; Accepted 9 June 2024
Available online 12 June 2024

To model pattern formation on mammalian skin in 1952 Alan Turing [31] presented his theory through reaction–diffusion (RD) equations. Bard stated that the size of the domain plays a crucial role in the emergence of spatial patterns [2]. Later, numerous studies have been conducted to produce spatial patterns with variations in domain size using RD equations. For example, Crampin et al. [6] used the concept of frequency-doubling to study the effect of isotropic domain growth in one spatial dimension for generating specific waveforms using RD models. The authors in [28] used a generalized Turing model with an alternating direction-implicit (ADI) scheme to study cell growth and pattern formation on the skin of growing marine angelfish. Neville et al. [27] considered both exponential domain growth and chemically controlled growth to investigate pattern formation in biological systems using Turing instability theory [32]. They discovered that domain growth or shrinkage depends quadratically on the pattern amplitude. Kim et al. [14] investigated how domain growth in a two-dimensional system influences zebra stripe development. They employed the Laplace–Beltrami operator on a triangulated surface within the RD system, varying rotational speeds to stretch and split the stripes, and resulting in diverse shapes, sizes, and brightness as the domain expanded. Liu et al. [21] used different waveforms with distinct speeds to produce various patterns in one and two-dimensional systems. They generated stripes with two phases (dark and light) in two-dimensional systems by using the theory of Turing instability in the growing domain. Furthermore, Krause et al. [16] extended previous work [21] by using concentration-dependent growth into various RD models to generate patterns in one-dimensional and N-dimensional manifolds for time-dependent expansion or contraction of space. Notably, although the study comprehensively investigated stripe patterns in 1D systems for FitzHugh–Nagumo kinetics under different growth scenarios, the production of fading patterns was not observed in either [21] or [16]. Yang and Kim [35] employed distinct space-dependent parameters within various domains to model realistic non-uniform zebra stripes, which enabled them to generate stripes of varying widths corresponding to different parts of the zebra' body. When parameters are kept constant [20], regular pattern formations can be modeled; however, mammals often exhibit regional variation in stripe spacing [15]. To simulate stripe pattern formations with nonhomogeneous thickness in a zebra, the authors took space-dependent diffusion and feed concentration parameters as the stripe spacing in zebras varies regionally. The authors achieved sharp transitions and smooth profiles in the RD system by applying an explicit finite difference scheme.

From the literature, numerous studies have investigated zebra stripe formation in two phases (dark and light) [8,10,11,23,30] but there has been no study on faded patterns, such as those seen in Equus burchelli [11]. The aim of this research is to explore the formation of faded stripes resembling zebra skin patterns in Equus burchelli using the Lengyel–Epstein model. We perform numerical investigations on the formations of multiple intense zebra stripes using an extending domain. We analyze the equilibrium state of the governing system in one-dimensional static domains, considering various frequency modes. By using the numerical data from these domains, we obtain the initial state for determining the required growth rate for forming multiple intense zebra stripes in one-dimensional expanding domains. Additionally, we perform convergence tests to assess the convergency of the numerical scheme for the governing system. Finally, we demonstrate the formation of multiple intense zebra stripes in two-dimensional expanding domains and on evolving curved surfaces through numerical simulations.

The research is structured as follows: Section 2 introduces the governing system used to mathematically model the formation of multiple intense zebra stripes. In Sections 3 and 5, the numerical solution algorithms for the governing equations are presented. Sections 4 and 6 show the numerical results obtained from the proposed algorithm. Finally, in Section 7, concluding remarks are provided.

2. Governing system

This research employs the Lengyel–Epstein model [20] to investigate the formation of multiple intense stripes in zebras:

$$\frac{\partial u(\mathbf{x},t)}{\partial t} = D_u \Delta u(\mathbf{x},t) + f(u(\mathbf{x},t), v(\mathbf{x},t)), \tag{1}$$

$$\frac{\partial v(\mathbf{x},t)}{\partial t} = D_v \Delta v(\mathbf{x},t) + g(u(\mathbf{x},t), v(\mathbf{x},t)), \tag{2}$$

where

$$f(u(\mathbf{x},t), v(\mathbf{x},t)) = k_1 \left(v(\mathbf{x},t) - \frac{u(\mathbf{x},t)v(\mathbf{x},t)}{1+v(\mathbf{x},t)^2} \right), \tag{3}$$

$$g(u(\mathbf{x},t), v(\mathbf{x},t)) = k_2 - v(\mathbf{x},t) - \frac{4u(\mathbf{x},t)v(\mathbf{x},t)}{1+v(\mathbf{x},t)^2}. \tag{4}$$

Here, $u(\mathbf{x},t)$ and $v(\mathbf{x},t)$ represent two morphogens at spatial $\mathbf{x}$ in the domain Ω and temporal t, which are the concentrations of an inhibitor and an activator, respectively. The nonlinear functions $f(u(\mathbf{x},t), v(\mathbf{x},t))$ and $g(u(\mathbf{x},t), v(\mathbf{x},t))$ involve the chemical reactions of $u(\mathbf{x},t)$ and $v(\mathbf{x},t)$. The parameters D_u and D_v are the diffusion coefficients of $u(\mathbf{x},t)$ and $v(\mathbf{x},t)$, respectively; while k_1 and k_2 denote positive constants related to the feed concentrations. In this study, we use the following homogeneous Neumann boundary condition [19]:

$$\mathbf{n} \cdot \nabla u(\mathbf{x},t) = 0 \text{ and } \mathbf{n} \cdot \nabla v(\mathbf{x},t) = 0, \ \mathbf{x} \in \partial\Omega, \tag{5}$$

where $\partial\Omega$ is the boundary of the domain and $\mathbf{n}$ is the unit outer normal to the boundary. The solutions of the governing Eqs. (1) and (2) at homogeneous steady state are given by $f(u^*, v^*) = 0$ and $g(u^*, v^*) = 0$, where

$$u^* = 1 + 0.04k_2^2 \text{ and } v^* = 0.2k_2. \tag{6}$$

Fig. 1. (a) Photo of baby and adult Equus burchelli type zebras. (b) and (c) are subparts of image (a).
Source: This photo is reproduced courtesy of *Frans van Heerden*.

These solutions correspond to the case where the concentrations of u and v cannot change with time. We shall use the above-mentioned conditions to simulate the formation of multiple intense stripes in zebras. The real shadow stripe patterns on Equus burchelli zebra-type skin can be seen in Fig. 1. It can be inferred that this shadow stripe pattern is dull in brightness when it is a baby zebra, however becomes darker as it grows into an adult zebra.

3. Numerical solution algorithm in one-dimensional space

In this section, we present a numerical approach for solving the governing system in one-dimensional space on the interval $\Omega = (L_x, R_x)$. We introduce the discrete domain $\Omega_d = \{x_i \mid x_{i+1} = x_i + h_i,\ 1 \le i < N_x,\ x_1 = L_x,\ x_{N_x} = R_x\}$, where h_i represents a non-uniform grid size and N_x denotes the total number of grids in the x-direction. Let T denote the final time, and N_t represents the number of temporal steps. Then, we denote by $u_i^n = u(x_i, n\Delta t)$ and $v_i^n = v(x_i, n\Delta t)$ where $\Delta t = T/N_t$ is the temporal step. We discretize the governing system (1) and (2) using an explicit finite difference method [9] with the following equations:

$$\frac{u_i^{n+1} - u_i^n}{\Delta t} = D_u \Delta_d u_i^n + k_1 \left(v_i^n - \frac{u_i^n v_i^n}{1 + (v_i^n)^2} \right), \tag{7}$$

$$\frac{v_i^{n+1} - v_i^n}{\Delta t} = D_v \Delta_d v_i^n + k_2 - v_i^n - \frac{4 u_i^n v_i^n}{1 + (v_i^n)^2}, \tag{8}$$

where

$$\Delta_d u_i^n = \frac{2}{h_{i-1}(h_{i-1} + h_i)} u_{i-1}^n - \frac{2}{h_{i-1} h_i} u_i^n + \frac{2}{h_i (h_{i-1} + h_i)} u_{i+1}^n$$

and

$$\Delta_d v_i^n = \frac{2}{h_{i-1}(h_{i-1} + h_i)} v_{i-1}^n - \frac{2}{h_{i-1} h_i} v_i^n + \frac{2}{h_i (h_{i-1} + h_i)} v_{i+1}^n.$$

We set $h_0 = h_1$ and $h_{N_x} = h_{N_x - 1}$ for the homogeneous Neumann boundary condition in one-dimensional space, and

$$u_0^n = u_2^n,\ u_{N_x+1}^n = u_{N_x-1}^n,\ v_0^n = v_2^n,\ \text{and}\ v_{N_x+1}^n = v_{N_x-1}^n. \tag{9}$$

We note that we use a fully explicit finite difference method for simplicity in exposition and to focus on the novel proposed model. We may use an unconditionally stable numerical scheme that does not have temporal step size restrictions [29] or a practically stable numerical method [18].

4. Numerical experiments in one-dimensional space

4.1. Equilibrium state in 1D static domains

We shall perform the numerical simulation to find the equilibrium state for the RD system (1) and (2) in the one-dimensional static domain [0, 10]. Here, the parameters are set as $N_x = 300$, $D_u = 1$, $D_v = 0.007$, $k_1 = 30$, $k_2 = 11$. First, we solve the discretized governing system (7) and (8) with the following initial states:

$$u(x, 0) = u^* + 0.05 \cos(kx), \quad v(x, 0) = v^* + 0.05 \cos(kx),$$

where $u^* = 1 + 0.04k_2^2$ and $v^* = 0.2k_2^2$ for $12 \le k \le 18$.

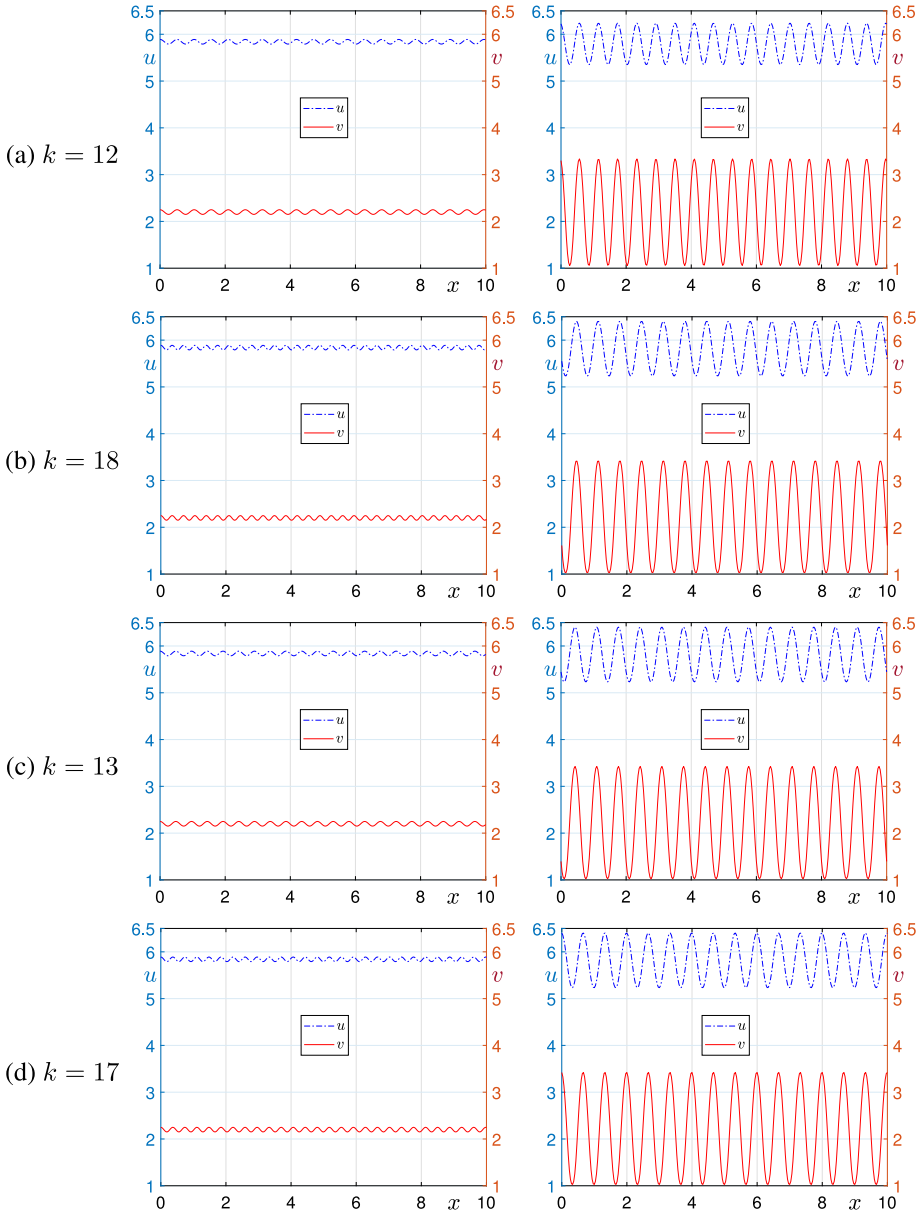

Fig. 2. Find the equilibrium state for (a) $k = 12$, (b) $k = 18$, (c) $k = 13$ and (d) $k = 17$; The first column shows initial states and second column shows equilibrium states at $t = 10000000\Delta t$.

Figs. 2 and 3 show initial states in first columns, and the equilibrium states in second columns for $12 \leq k \leq 18$. At $t = 10^7\Delta t$, each number of frequency modes has the same number of frequency mode as $k = 15$. Therefore, we plan to save this numerical data of equilibrium state for $k = 15$ at $t = 10^7\Delta t$ and load it separately to analyze the growth factor of evolving domains that can form faded patterns.

4.2. Growth factors for fade pattern formation in 1D evolving domains

Now, we shall find a suitable growth speed value in the x-direction to form fading patterns in one-dimensional evolving domains. First, the initial condition is set by loading the equilibrium state shown in Fig. 3(f). Next, we use the evolving condition $x(t + \Delta t) = \left(1 + s\frac{t}{100000\Delta t}\right)x(0)$. If the growth speed values are $s = 0.5$, $s = 0.8$, $s = 0.9$, and $s = 1.0$, the numerical results in

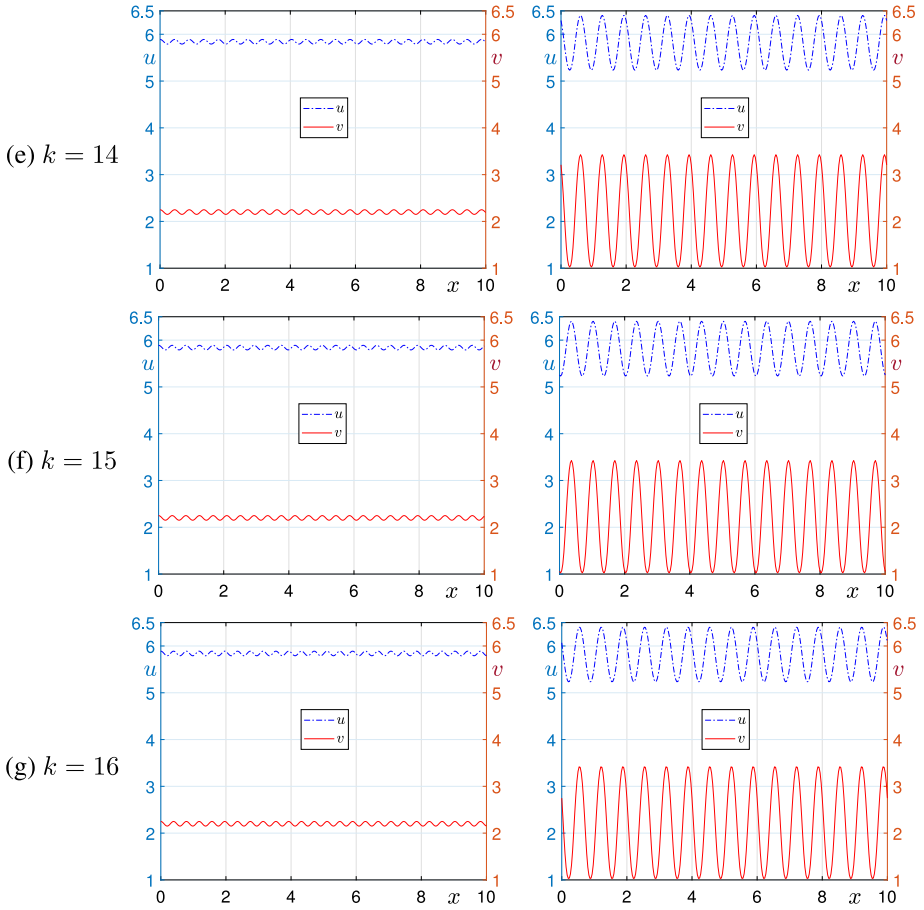

Fig. 3. Find the equilibrium state for (e) $k = 14$, (f) $k = 15$ and (g) $k = 16$; The first column shows initial states and second column shows equilibrium states at $t = 10000000\Delta t$.

Figs. 4(a), (b), (c) and (d) can be obtained. There are fade frequency perturbations between principal frequency perturbations. It is possible to form faded zebra stripe patterns in the two-dimensional (2D) evolving domains by applying the growth speed values about $0.8 \leq s \leq 1.0$. We shall save and recall the numerical results in Fig. 4 for visualization of continuously formation of faded zebra stripe patterns in 2D extending domains.

4.3. Visualization of continuously faded zebra stripe patterns in 2D extending domains

To visualize continuously fading zebra stripe patterns in 2D expanding domains, we refer back to the 1D numerical results presented in Fig. 4. Firstly, these numerical results in Fig. 4 are extended into the y-direction while maintaining the same frequency values. Secondly, using a grayscale color scheme ranging from white (lower values) to black (higher values), we plot these extended numerical results of u (see Fig. 5) in 2D expanding domains. As shown in Fig. 5, the 1D numerical results are plotted in 2D expanding domains for various growth factor values: (a) $s = 0.8$, (b) $s = 0.9$ m and (c) $s = 1.0$.

In previous studies related to the effects of domain growth, Maini et al. [24] considered an exponentially growing domain, a linearly growing domain and a logistically growing domain to numerically research period-doubling patterns. In their numerical results as shown in Fig. 6, there are two phases states. In contrast, in our numerical results in Fig. 5, three phases (gray scale) appear using an appropriate growth rate s. With a suitable growth rate value s, the faded stripe patterns of a zebra can be simulated.

4.4. Convergence experiments

To investigate whether the parameter values used in the simulation were sufficiently small, we compared the simulation results in Fig. 5(d) using parameter values that were halved for both spatial and temporal resolutions. Fig. 7(a) shows the same result of Fig. 5(d). We consider the same conditions as those in Fig. 5(d) except for N_x and Δt. Fig. 7(b) is a result using $N_x = 600$ and $\Delta t = 5.5556\text{e-}5$. Even with parameters halved, the results are not different.

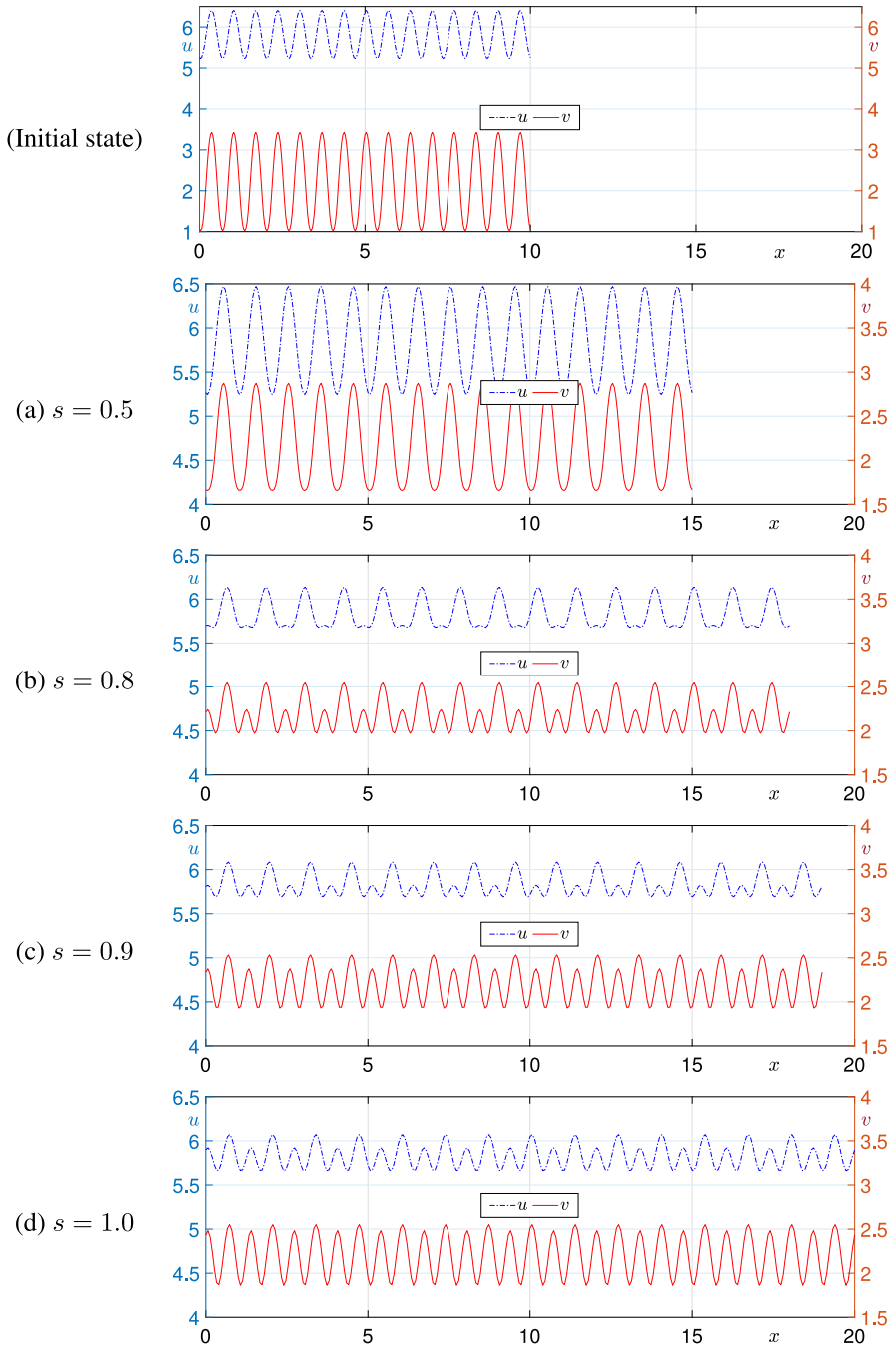

Fig. 4. Finding the growth factor using the equilibrium state in Fig. 3(f). The snapshots of u (blue color) and v (red color) for each growth factor (a) $s = 0.5$, (b) $s = 0.8$, (c) $s = 0.9$ and (d) $s = 1.0$ at $t = 100000\Delta t$. (For interpretation of the references to color in this figure legend, the reader is referred to the web version of this article.)

4.5. Faded zebra stripe pattern formation using multi-speed growth rates

From now on, we shall numerically investigate the formation of faded zebra stripe patterns under multi-speed growth rate conditions. Let us consider the multi-speed growth rates s defined by $s_{\max} = 1.0$ and $s_{\min} = 0.5$ as follows:

$$s_i = s_{\min} + \frac{s_{\max} - s_{\min}}{2}\left(1 + \tanh\left(\frac{x_i^n - x_{\frac{N_x}{5}}^n}{5\sqrt{2}}\right)\right),$$

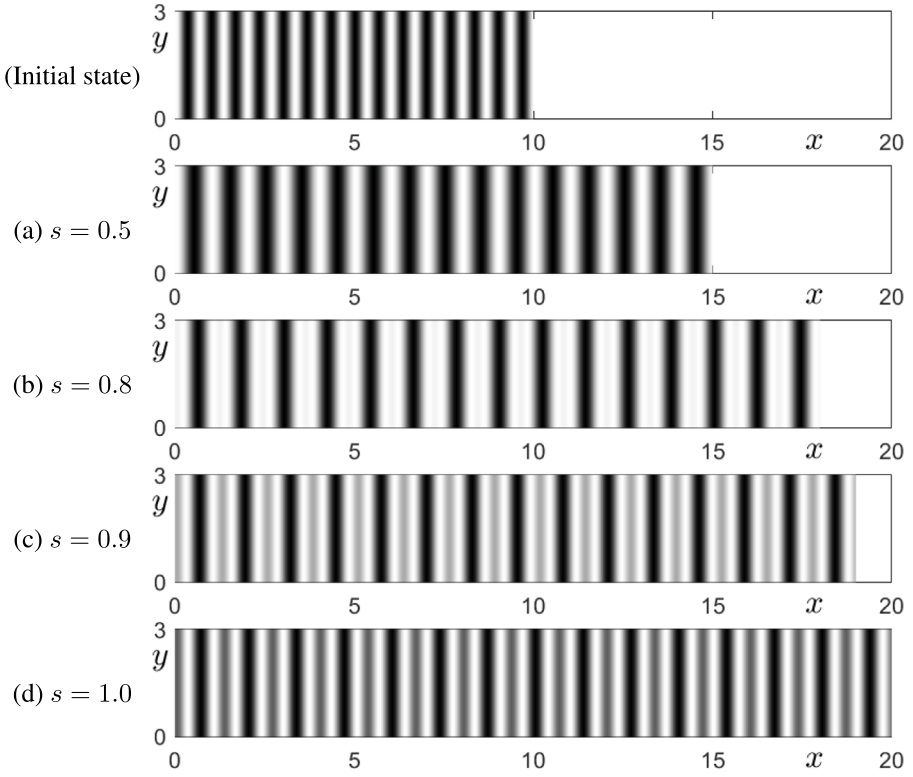

Fig. 5. Faded zebra stripe patterns for inhibitor u in 2D extending domains at $t = 100000\Delta t$, with respect to different growth factor values (a) $s = 0.5$, (b) $s = 0.8$, (c) $s = 0.9$ and (d) $s = 1.0$.

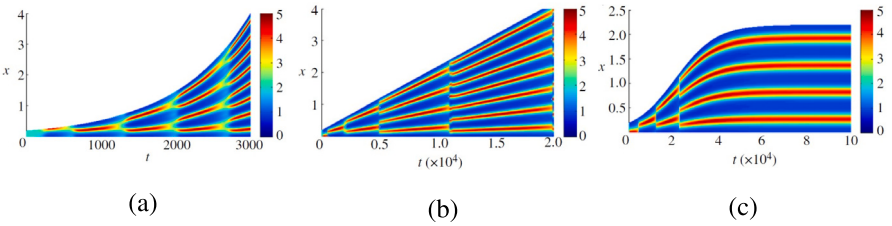

Fig. 6. Turing patterns for the Schnakenberg kinetics on growing domain under conditions of (a) exponential growth, (b) linear growth, and (c) logistical growth. *Source:* Reprinted from Maini et al. [24] with permission from the Royal Society publishing.

where $N_x = 300$, and $i = 0, \ldots, N_x - 1$. Let h_i^0 be initial spatial step size. In this experiment, we use the evolving condition: $h_i^n = \left(1 + s_i \frac{n}{100000}\right) h_i^0$. The discrete domain is updated as $\Omega_d^n = \{x_i^n | x_{i+1}^n = x_i^n + h_i^n, 0 \le i \le N_x\}$. The initial state is used as the initial state of Fig. 5. Fig. 8 shows the numerical result of u at $t = 100000\Delta t$. As shown in the faded stripe patterns with different brightness formed from the belly to the buttocks of the zebra in Fig. 1(c), the numerical results in Fig. 8 also show that the faded stripe patterns with different brightness are formed depending on the multi-speed growth rates. The rationale for using the hyperbolic tangent profile for growth rate is explained as follows: during the growth process of a zebra from the torso to the buttocks, stretching at the front of the torso progresses slowly, while growth accelerates in the middle part, leading to the creation of another transition layer. The growth process progresses at a uniform rate as it proceeds toward the buttocks.

5. Numerical solution algorithm on a curved surface in 3D space

Next, let us extend the Lengyel–Epstein model (1) and (2) by incorporating the Laplace–Beltrami operator Δ_S:

$$\frac{\partial u(\mathbf{x},t)}{\partial t} = D_u \Delta_S u(\mathbf{x},t) + k_1 \left(v(\mathbf{x},t) - \frac{u(\mathbf{x},t)v(\mathbf{x},t)}{1 + v(\mathbf{x},t)^2} \right), \tag{10}$$

$$\frac{\partial v(\mathbf{x},t)}{\partial t} = D_v \Delta_S v(\mathbf{x},t) + k_2 - v(\mathbf{x},t) - \frac{4u(\mathbf{x},t)v(\mathbf{x},t)}{1 + v(\mathbf{x},t)^2}, \tag{11}$$

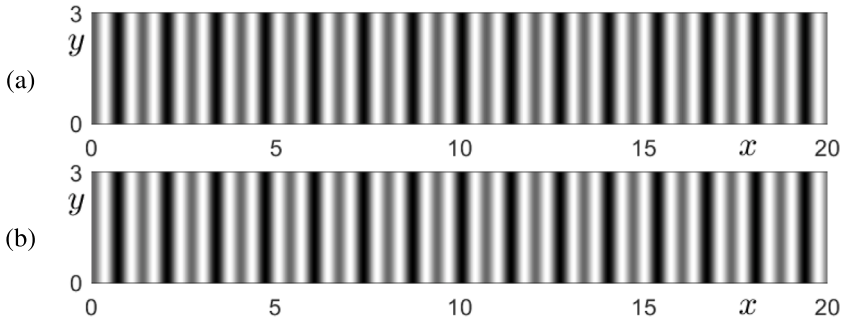

Fig. 7. Faded zebra stripe patterns for u with (a) $N_x = 300$, $\Delta t = 1.1111\text{e-}4$ and (b) $N_x = 600$, $\Delta t = 5.5556\text{e-}5$, respectively.

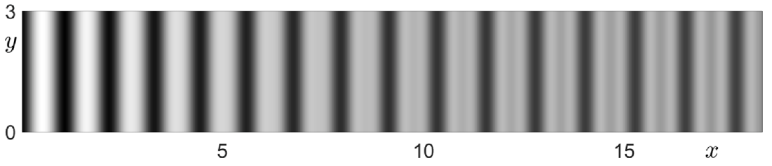

Fig. 8. Faded zebra stripe patterns for inhibitor u in 2D extending domain at $t = 100000\Delta t$ using multi-speed growth rates.

where $\mathcal{S}$ is a given curved surface domain, $\mathbf{x} \in \mathcal{S}$ and $t > 0$. The description of the discretization for the surface Lengyel–Epstein model (10) and (11) proceeds as follows. On a triangular surface mesh M of a closed smooth surface $\mathcal{S}$ as shown in Fig. 9(a), the surface vertex set $\{\mathbf{x}\}_{i=1}^{N}$ including N points is defined as follows. The one-ring neighbors surface vertex indices set is defined as $V(i) = \{i_1, i_2, \ldots, i_m\}$, which holds $i_1 = i_m$ for a surface vertex $\mathbf{x}_i$ as seen in Fig. 9(b). The surface vertices $\mathbf{x}_i$, $\mathbf{x}_{j_-}$ and $\mathbf{x}_j$ constitute a triangle T_j. The summation of areas $A(\mathbf{x}_i)$ for each triangle T_j around surface vertex $\mathbf{x}_i$ is defined as follows [13,34]:

$$A(\mathbf{x}_i) = \sum_{j \in V(i)} \frac{\sqrt{\|\mathbf{x}_j - \mathbf{x}_i\|^2 \|\mathbf{x}_{j_+} - \mathbf{x}_i\|^2 - \left(\mathbf{x}_j - \mathbf{x}_i, \mathbf{x}_{j_+} - \mathbf{x}_i\right)^2}}{2}.$$

The representations $u(\mathbf{x}_i, n\Delta t)$ and $v(\mathbf{x}_i, n\Delta t)$ are simply denoted by u_i^n and v_i^n, respectively. The discretized Laplace–Beltrami operators [33] can be obtained using the curvature normal formula [25] as follows:

$$\begin{aligned} \Delta_{\mathcal{S}} u_i &\approx \frac{3}{A(\mathbf{x}_i)} \sum_{j \in V(i)} \frac{\cot\theta_{ij} + \cot\theta_{ij_+}}{2}(u_j - u_i), \\ \Delta_{\mathcal{S}} v_i &\approx \frac{3}{A(\mathbf{x}_i)} \sum_{j \in V(i)} \frac{\cot\theta_{ij} + \cot\theta_{ij_+}}{2}(v_j - v_i), \end{aligned} \tag{12}$$

where angles θ_{ij} and θ_{ij_+} in triangles T_{j+} and T_j can be seen in Fig. 9(c), respectively. Using the above mentioned descriptions of the discretization, we have a discretized evolutionary system using the explicit Euler's method for the surface Lengyel–Epstein model (10) and (11) as follows:

$$\frac{u_i^{n+1} - u_i^n}{\Delta t} = D_u \Delta_{\mathcal{S}} u_i^n + k_1 \left(v_i^n - \frac{u_i^n v_i^n}{1 + (v_i^n)^2} \right), \tag{13}$$

$$\frac{v_i^{n+1} - v_i^n}{\Delta t} = D_v \Delta_{\mathcal{S}} v_i^n + k_2 - v_i^n - \frac{4 u_i^n v_i^n}{1 + (v_i^n)^2}. \tag{14}$$

6. Numerical experiments on evolving curved surfaces in 3D space

On the evolving curved surfaces (in details evolving conditions, see [12,14]), we shall perform the investigation *in silico* for formations of faded zebra stripe patterns. The initial states are set as shown in Fig. 10(a):

$$\begin{aligned} u(\mathbf{x}, 0) &= u^* - 5.8\cos(2kL) \\ v(\mathbf{x}, 0) &= v^* - 2.2\cos(2kL), \end{aligned}$$

where $u^* = 1 + 0.04k_2^2$, $v^* = 0.2k_2$, $L = R\theta$, R is a radius of initial sphere and θ is a rotation angle of a triangular curved surface. The parameters are used as $\Delta t = 0.001$, $D_u = 1$, $D_v = 0.007$, $k_1 = 30$ and $k_2 = 11$.

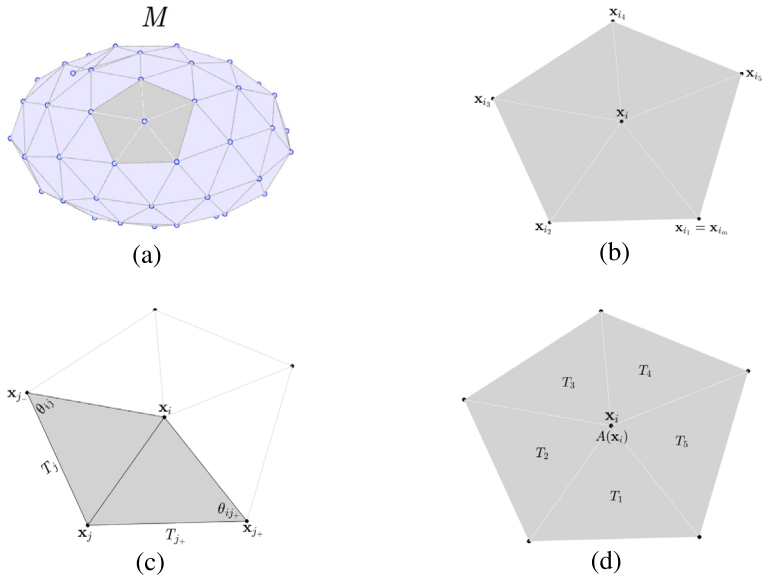

Fig. 9. Schematic illustrations. (a) triangular surface, (b) surface vertices set of one-ring neighbors of $\mathbf{x}_i$ with $\mathbf{x}_{i_1} = \mathbf{x}_{i_m}$, (c) triangles T_j and T_{j+} including angles θ_{ij} and θ_{ij_+}, and (d) area $A(\mathbf{x}_i)$ at vertex $\mathbf{x}_i$.

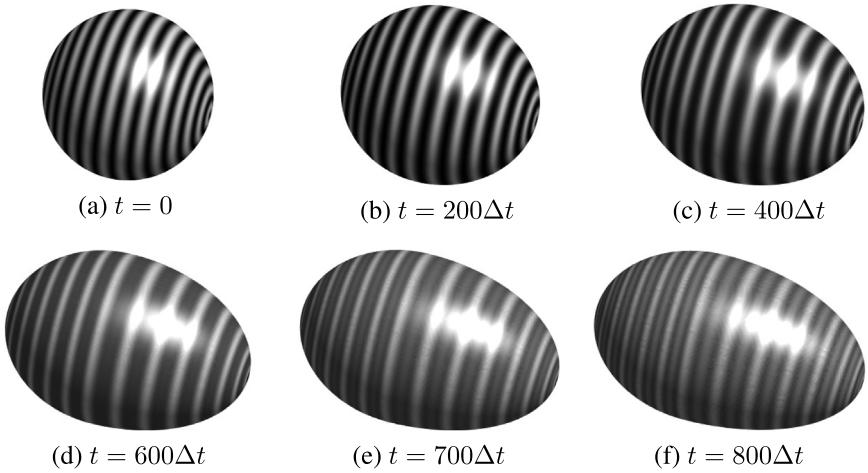

Fig. 10. Faded zebra stripe pattern formation on evolving curved surfaces.

The process of forming faded zebra stripe patterns on evolving curved surfaces can be seen in Figs. 10(b)–(f). The numerical behaviors shown in Figs. 10(b) and (c) do not exhibit a change in pattern; however, a change in scale begins to emerge in the results shown in Fig. 10(d), and faded zebra stripe patterns can be observed in the results shown in Figs. 10(e) and (f). The number of dark stripes identified in the final numerical results is approximately 27∼28, which is consistent with the number of stripe formation (about ∼26) of Equus burchelli-type zebras as presented in [3]. These numerical results also support the choice of a frequency mode $k = 15$ in the initial conditions.

7. Conclusions

An *in silico* investigation of the formation of multiple intense zebra stripes using extending domains was conducted. The Lengyel–Epstein model was employed and discretized to describe a numerical method in the one-dimensional space. The explicit Euler method was applied to numerically solve the proposed model. Various numerical experiments were demonstrated to find the equilibrium state, appropriate growth factor s and convergence. Convergence experiments were conducted for both space and time by changing the spatial and temporal step sizes. It was validated that consistent numerical results were obtained despite changes in the spatial and temporal step sizes. To show the faded zebra stripes as shown in Figs. 1(b) and (c), the computational results from the 1D

domain were visualized in 2D by extending the domains. In the latter part of this research, numerical experiments on evolving curved surfaces were conducted. The proposed method successfully reproduced the numerical behaviors observed in 1D space when applied to evolving curved surfaces, resulting in patterns resembling zebra stripes (approximately 26 stripes) with some faded stripes as described in [3]. Future research will use stable numerical schemes [1] to further enhance the performance of the proposed algorithm. Moreover, to simulate full-scale zebra pattern formation, we will incorporate curvature-dependent parameters [17].

CRediT authorship contribution statement

Hyundong Kim: Conceptualization, Data curation, Formal analysis, Funding acquisition, Investigation, Methodology, Project administration, Resources, Software, Validation, Visualization, Writing – original draft, Writing – review & editing. **Jyoti:** Investigation, Resources, Validation, Writing – original draft. **Soobin Kwak:** Investigation, Validation, Writing – original draft, Writing – review & editing, Visualization. **Seokjun Ham:** Investigation, Resources, Software, Validation, Visualization, Writing – original draft, Writing – review & editing. **Junseok Kim:** Conceptualization, Formal analysis, Funding acquisition, Investigation, Methodology, Project administration, Supervision, Validation, Writing – original draft, Writing – review & editing.

Declaration of competing interest

The authors declare that they have no known competing financial interests or personal relationships that could have appeared to influence the work reported in this paper.

Data availability

Data will be made available on request.

Use of AI tools declaration

The authors have not used Artificial Intelligence (AI) tools in the creation of this article.

Acknowledgments

The first author (Hyundong Kim) was supported by Basic Science Research Program through the National Research Foundation of Korea (NRF) funded by the Ministry of Education, Korea (NRF-2020R1A6A3A13077105). The corresponding author (J.S. Kim) was supported by the Brain Korea 21 FOUR through the National Research Foundation of Korea funded by the Ministry of Education of Korea. The authors are grateful to the referees whose detailed comments on our manuscript have greatly improved the paper.

References

[1] H. Banda, M. Chapwanya, P. Dumani, Pattern formation in the Holling–Tanner Predator–Prey model with predator-taxis, A nonstandard finite difference approach, Math. Comput. Simul. 196 (2022) 336–353.
[2] J.B. Bard, A model for generating aspects of zebra and other mammalian coat patterns, J. Theoret. Biol. 93 (2) (1981) 363–385.
[3] J.B. Bard, Modelling speciation: Problems and implications, in: In Silico Biology, Vol. 15, (1–2) 2023, pp. 23–42.
[4] A. Cabrera, Subspecific and individual variation in the Burchell zebras, J. Mammal. 17 (2) (1936) 89–112.
[5] T. Caro, A. Izzo, R.C. Reiner Jr., H. Walker, T. Stankowich, The function of zebra stripes, Nature Commun. 5 (1) (2014) 3535.
[6] E.J. Crampin, E.A. Gaffney, P.K. Maini, Reaction and diffusion on growing domains: Scenarios for robust pattern formation, Bull. Math. Biol. 61 (1999) 1093–1120.
[7] C. Darwin, The Variation of Animals and Plants Under Domestication, Vol. 2, John Murray, 1868.
[8] C.P. Gravan, R. Lahoz-Beltra, Evolving morphogenetic fields in the zebra skin pattern based on Turing's morphogen hypothesis, Int. J. Appl. Math. Comput. Sci. 14 (3) (2004) 351–361.
[9] S. Ham, J. Kim, Stability analysis for a maximum principle preserving explicit scheme of the Allen–Cahn equation, Math. Comput. Simulation 207 (2023) 453–465.
[10] D. Jeong, Y. Li, Y. Choi, M. Yoo, D. Kang, J. Park, J. Choi, J. Kim, Numerical simulation of the zebra pattern formation on a three-dimensional model, Phys. A 475 (2017) 106–116.
[11] B.B. Jonathan, A unity underlying the different zebra striping patterns, J. Zool. 183 (4) (1977) 527–539.
[12] H. Kim, Explicit Time-Stepping Approach for Pattern Formation on Evolving Curved Surfaces (Ph.D. dissertation), Korea University, 2022.
[13] H. Kim, S. Kang, G. Lee, S. Yoon, J. Kim, Shape transformation on curved surfaces using a phase-field model, Commun. Nonlinear Sci. Numer. Simul. 133 (2024) 107956.
[14] H. Kim, A. Yun, S. Yoon, C. Lee, J. Park, J. Kim, Pattern formation in reaction–diffusion systems on evolving surfaces, Comput. Math. Appl. 80 (9) (2020) 2019–2028.
[15] S. Kondo, The reaction–diffusion system: a mechanism for autonomous pattern formation in the animal skin, Genes Cells 7 (2002) 535–541.
[16] A.L. Krause, E.A. Gaffney, B.J. Walker, Concentration-dependent domain evolution in reaction-diffusion systems, Bull. Math. Biol. 85 (2) (2023) 14.
[17] S. Kwak, J. Yang, J. Kim, A conservative Allen–Cahn equation with a curvature-dependent Lagrange multiplier, Appl. Math. Lett. 126 (2022) 107838.
[18] C. Lee, Y. Choi, J. Kim, An explicit stable finite difference method for the Allen–Cahn equation, Appl. Numer. Math. 182 (2022a) 87–99.
[19] C. Lee, J. Park, S. Kwak, S. Kim, Y. Choi, S. Ham, J. Kim, An adaptive time-stepping algorithm for the Allen–Cahn equation, J. Funct. Space (2022b) 2022.
[20] I. Lengyel, I.R. Epstein, Modeling of turing structure in the Chlorite–Iodide–Malonic acid–Starch reaction system, Science 251 (4994) (1991) 650–652.
[21] Y. Liu, P.K. Maini, R.E. Baker, Control of diffusion-driven pattern formation behind a wave of competency, Phys. D 438 (2022) 133297.
[22] J.A. Lusis, Striping patterns in domestic horses, Genetica 23 (1943) 31–62.

[23] P.K. Maini, T.E. Woolley, The Turing Model for Biological Pattern Formation, Springer, New York, 2019, pp. 189–204.
[24] P.K. Maini, T.E. Woolley, R.E. Baker, E.A. Gaffney, S.S. Lee, Turing's model for biological pattern formation and the robustness problem, Interface Focus 2 (4) (2012) 487–496.
[25] M. Meyer, M. Desbrun, P. Schröder, A.H. Barr, Discrete Differential-Geometry Operators for Triangulated 2-Manifolds, Springer, Berlin, Heidelberg, 2003, pp. 35–57.
[26] A. Muhl-Richardson, M.G. Parker, G. Davis, How the Zebra got its Rump Stripes: Salience at Distance and in Motion, 2021, bioRxiv. 2021–04.
[27] A.A. Neville, P.C. Matthews, H.M. Byrne, Interactions between pattern formation and domain growth, Bull. Math. Biol. 68 (2006) 1975–2003.
[28] K.J. Painter, P.K. Maini, H.G. Othmer, Stripe formation in juvenile pomacanthus explained by a generalized turing mechanism with chemotaxis, Proc. Natl. Acad. Sci. 96 (10) (1999) 5549–5554.
[29] J. Park, C. Lee, Y. Choi, H.G. Lee, S. Kwak, Y. Hwang, J. Kim, An unconditionally stable splitting method for the Allen–Cahn equation with logarithmic free energy, J. Engrg. Math. 132 (1) (2022) 18.
[30] S.M. Rasheed, Pattern formation for a new model of reaction–diffusion system, in: 2018 International Conference on Advanced Science and Engineering, ICOASE, 2018, pp. 99–104.
[31] A.M. Turing, The chemical basis of morphogenesis, Phil. Trans. Roy. Soc. Lond. 237 (641) (1952) 37–72.
[32] D. Wu, Y. Yang, P. Wu, Impacts of prey-taxis and nonconstant mortality on a spatiotemporal Predator–Prey system, Math. Comput. Simulation 208 (2023) 283–300.
[33] G. Xu, Convergence of discrete Laplace–Beltrami operators over surfaces, Comput. Math. Appl. 48 (3) (2004a) 347–360.
[34] G. Xu, Discrete Laplace–Beltrami operators and their convergence, Comput. Aided Geom. Design 21 (8) (2004b) 767–784.
[35] J. Yang, J. Kim, Computer simulation of the nonhomogeneous zebra pattern formation using a mathematical model with space-dependent parameters, Chaos Solitons Fractals 169 (2023) 113249.